Title

Key Amino Acid Residues of Mitochondrial Transcription Factor A Synergize with Abasic (AP) Site Dynamics To Facilitate AP-Lyase Reactions.

Journal

ACS Chemical Biology, 18(5)

Authors

Zhao, Wenxin

Xu, Wenyan

Tang, Jin

et al.

Publication Date

2023-05-19

DOI

10.1021/acschembio.3c00047

Peer reviewed

HHS Public Access

Author manuscript

ACS Chem Biol. Author manuscript; available in PMC 2024 May 19.

Published in final edited form as:

ACS Chem Biol. 2023 May 19; 18(5): 1168–1179. doi:10.1021/acschembio.3c00047.

The Key Amino Acid Residues of Mitochondrial Transcription Factor A (TFAM) Synergize with Abasic (AP) Site Dynamics to Facilitate AP-Lyase Reactions

Wenxin Zhao[1], **Wenyan Xu**[1], **Jin Tang**[1], **Shivansh Kaushik**[1], **Chia-En A. Chang**[1,2], **Linlin Zhao**[1,2,*]

[1]Department of Chemistry, University of California, Riverside, Riverside, California, 92521, United States

[2]Environmental Toxicology Graduate Program, University of California, Riverside, Riverside, California, 92521, United States

Abstract

Human mitochondrial DNA (mtDNA) encodes 37 essential genes and plays a critical role in mitochondrial and cellular functions. mtDNA is susceptible to damage by endogenous and exogenous chemicals. Damaged mtDNA molecules are counteracted by the redundancy, repair, and degradation of mtDNA. In response to difficult-to-repair or excessive amounts of DNA lesions, mtDNA degradation is a crucial mitochondrial genome maintenance mechanism. Nevertheless, the molecular basis of mtDNA degradation remains incompletely understood. Recently, mitochondrial transcription factor A (TFAM) has emerged as a factor in degrading damaged mtDNA containing abasic (AP) sites. TFAM has AP-lyase activity, which cleaves DNA at AP sites. Human TFAM and its homologs contain a higher abundance of Glu than that of the proteome. To decipher the role of Glu in TFAM-catalyzed AP-DNA cleavage, we constructed TFAM variants and used biochemical assays, kinetic simulations, and molecular dynamics (MD) simulations to probe the functional importance of E187 near a key residue K186. Our previous studies showed that K186 is a primary residue to cleave AP-DNA via Schiff base chemistry. Here, we demonstrate that E187 facilitates β-elimination, key to AP-DNA strand scission. MD simulations showed that extrahelical confirmation of the AP lesion and the flexibility of E187 in TFAM-DNA complexes facilitate AP-lyase reactions. Together, highly abundant Lys and Glu residues in TFAM promote AP-DNA strand scission, supporting the role of TFAM in AP-DNA turnover and implying the breadth of this process across different species.

*To whom correspondence should be addressed. Tel: 1-951-827-9081; linlin.zhao@ucr.edu.

Supporting Information

The Supporting Information is available free of charge at

Figures describing the TFAM-DNA binding and kinetic assays; Tables summarizing the abundance of TFAM and kinetic and simulation data.

The authors declare no competing financial interest.

INTRODUCTION

In higher eukaryotes, mitochondria are essential subcellular organelles for energy production, metabolism, and signaling.[1] Mitochondrial DNA (mtDNA) encodes 13 protein subunits of the oxidative phosphorylation system and a set of tRNAs and rRNAs. Compared to nuclear DNA (nDNA), mtDNA is more susceptible to chemical modifications by endogenous and exogenous factors partly due to its proximity to the oxidative phosphorylation system and the lack of certain DNA repair pathways.[2-4] Unrepaired DNA lesions, point mutations, and deletions in the mitochondrial genome contribute to the heterogeneity of mtDNA, also known as mtDNA heteroplasmy, which has been implicated in mitochondrial diseases, neurodegeneration, and cancer.[5, 6] mtDNA damage is counteracted by a robust mitochondrial base excision repair system, its multi-copy characteristic, and rapid mtDNA turnover,[2, 7, 8] which occur in the context of mitochondrial dynamics and mitophagy.[9] The systems to protect mtDNA also include scavengers of reactive oxygen species, such as superoxide dismutase and mitochondrial glutathione peroxidase 1.[10] Notably, when cultured cells or experimental animals are exposed to genotoxic chemicals, damaged mtDNA molecules are quickly degraded upon genotoxic stress without an increase in the mutation load.[9, 11, 12] Even under unstressed conditions, the half-life of mtDNA is only in a matter of days.[13] The mtDNA copy number fluctuates in a given tissue and varies considerably based on the cell and tissue types.[7] Furthermore, the degraded mtDNA fragments are known to translocate to the cytoplasm and trigger immunological pathways.[3, 14, 15] Together, the rapid turnover of mtDNA, its susceptibility to damage, and the functional importance of released mtDNA in immune responses have led to the proposed role of mtDNA as a cellular genotoxic stress sensor.[3]

Mechanistically, how damaged mtDNA molecules are degraded remains partially understood. A few enzymes have been shown to be involved in mtDNA degradation, including the exonuclease domain of DNA polymerase (pol) γ[16, 17], genome maintenance exonuclease 1 (MGME1)[16, 18] with controversies,[15, 19] and flap endonuclease 1 (FEN1).[15] Pol γ and MGME1 process mtDNA containing induced double-strand breaks into shorter fragments in mammalian cells and mouse models.[16-18] FEN1 has been implicated in promoting mtDNA fragment release into cytoplasm on the basis of reduced cytosolic mtDNA fragments upon silencing Fen1.[15] In addition, mitochondrial transcription factor A (TFAM) has emerged as a new player in mtDNA turnover.[20-22] As a key mtDNA-packaging protein, TFAM organizes mtDNA into DNA-protein complexes known as nucleoids.[23] Besides, TFAM is an essential factor in mtDNA transcription activation.[24, 25] Recently, TFAM has been shown to cleave DNA molecules containing abasic (AP) sites in vitro and in cells,[20, 21] arguing its role in damaged mtDNA turnover. AP sites are one of the most abundant DNA lesions in mtDNA and nDNA, present at a level of 1 AP lesion/10^5-10^6 nt.[26]

Key to the AP lyase activity of TFAM is its high Lys content (15% of the amino acid residues in the mature TFAM). A proximal Lys activates an AP lesion for β-elimination via Schiff-base chemistry to form single-strand breaks (SSBs).[20, 21] A body of literature in the DNA repair field has shown that for DNA glycosylases, the β-elimination step can be catalyzed by carboxylate-containing Glu or Asp residues (e.g., T4 endonuclease V[27]), primary or secondary amines (e.g., NEIL1[28], also reviewed in ref. 29). Similarly,

pol β uses E71 to perform a water-assisted H-abstraction at the C2′ position to achieve its dRp-lyase activity.[30] Historically, the effects of carboxylate-containing amino acid residues on the Schiff base intermediates have been extensively studied with rhodopsin systems.[31] Remarkably, the abundance of Glu (12%) in TFAM is much higher than its average abundance (6.9%) in the human proteome (Table S1), and such a high frequency is conserved in TFAM homologs from different species (Table S2). Intriguingly, more than half of these Glu residues in TFAM are present in KE clusters (Fig. 1B). Considering that multiple Lys residues can be involved in Schiff base formation with AP sites,[20, 21, 32] a proximal Glu would be able to facilitate β-elimination by the deprotonating the 2′ carbon atom of the sugar ring, or serving as a Schiff base counterion, or both. Yet, the potential contribution of the highly abundantly Glu residues to the AP-lyase activity of TFAM has not been explored.

Herein, we clarify the role of a Glu residue (E187) in TFAM-mediated AP-DNA cleavage using wet-lab experiments and computer simulations. E187 is chosen given its proximity to the hotspot K186 in TFAM-facilitated AP-lyase reactions.[20, 21, 32] We demonstrate that E187 facilitates β-elimination through detailed kinetic analysis and molecular dynamics (MD) simulations. Our kinetic assays and simulations show that TFAM E187A variant has a reduced rate of β-elimination. MD simulations revealed that AP sites in the TFAM-DNA complex exhibits both intrahelical and extrahelical conformations with the latter facilitating the Schiff base formation. Collectively, our data shed light on the importance of E187 in the TFAM-mediated AP-lyase reactions and provide a basis for understanding the high abundance of Glu in TFAM homologs and their role in mtDNA maintenance.

RESULTS

Design and validation of the Cys-null variant

We have demonstrated that Lys residues of TFAM are essential for catalyzing the DNA cleavage at AP sites via Schiff base chemistry (Fig. 1C).[20, 21] The resulting 3′-PUA (after β-elimination) reacts readily with C49 or C246 of TFAM to form (meta)stable DNA-protein cross-links (DPCs) via a Michael addition-type reaction.[21] To probe the role of key Lys and Glu residues without complications from Cys-derived DPCs, we prepared a Cys-null variant of TFAM (C49S/C246S, hereinafter referred to as 2CS), and verified that 2CS maintained similar properties relative to wild-type (wt) TFAM through the following experiments. In terms of DNA-binding activity, 2CS showed a slightly higher affinity with DNA, with a $K_{d,DNA}$ of 2.2 (± 0.2) nM, compared to a $K_{d,DNA}$ of 9.9 (± 1.4) nM for wt TFAM (Fig. S1A) based on fluorescence anisotropy measurements. Regarding the AP lyase activity, the rates of AP-DNA disappearance (k_{dis}) were 23 (± 2.3) x 10^{-5} s^{-1} and 18 (± 2.2) x 10^{-5} s^{-1} for 2CS and wt TFAM, respectively (Figs. 2A, 2B, S2A, S2B and Table 1). The overall percentage yield of DPCs was a bit lower for 2CS (71 %) compared to wt TFAM (83%) in a 12-h reaction. The lower yield of DPCs with 2CS is consistent with the lack of Cys-derived DPCs (Figs. 2A and 2B). We evaluated the stability of DPCs resulting from a 15-h reaction with wt TFAM or 2CS under the physiological pH (7.4) and ionic strength conditions. Although the relative abundance of DPCs from both reactions decreased over time, a faster decrease was observed with 2CS (Figs. S4A and S4C). This can be explained

by the presence of imine-based DPCs formed with 2CS, which are less stable than the Michael-type DPCs formed with wt TFAM.[21] Fitting the decrease of the DPC abundance over time to a single exponential decay function resulted in a half-life ($t_{1/2}$) of 7 h for 2CS (Fig. 2C) and 43 h for wt TFAM (Fig. 2D). Consistent with the poor thermostability of the Schiff base, DPCs derived from 2CS were more sensitive to heating. For example, the relative abundance of DPCs from 2CS was approximately 8% at 61 °C (Fig. 2E), whereas the relative abundance was approximately 20% for wt TFAM (Fig. 2F).

To verify that 2CS maintains the local interactions near the AP lesion in TFAM-DNA complexes, we identified amino acid residues of TFAM cross-linked to the AP lesion using tandem mass spectrometry (Fig. S5, Tables S4 and S5). Under *in situ* trapping by $NaBH_3CN$, the Schiff base intermediates formed between the AP lesion and a proximal Lys were captured. Mass spectrometry data show that the AP lesion cross-links primarily with K186 of 2CS. The relative abundance of K186-conjugated DPCs was 87% on the basis of semi-quantification using integrated peak areas. The abundance correlates nicely with an abundance of 85% with wt TFAM.[21] In the absence of $NaBH_3CN$, the AP lesion was cross-linked to a number of Lys residues, including K111 (36% relative abundance), K76 (26%), and K69 (15%). Interestingly, K111 also locates in a K111/E112 cluster in the primary sequence, as shown in Figure 1B. These results do not abrogate the importance of K186 because reactions in the presence of $NaBH_3CN$ should capture the predominant conformation in the initial phase of the reaction, whereas reaction products in the absence of $NaBH_3CN$ may represent thermodynamically stable products after reversible reactions with K186. The observed products are consistent with the conformational dynamics of TFAM-DNA complexes reported by others[33] and us.[32] For example, the TFAM-bound complex can undergo butterfly-like motions with the two HMG domains.[33] Together, these data confirm that similar local interactions were maintained with 2CS relative to wt TFAM and that 2CS is a suitable variant to probe the role of Glu in TFAM-mediated AP lyase reactions.

Probing the role of Glu using TFAM variants

The high abundance of Glu residues and their proximity to Lys residues prompted us to investigate their roles in TFAM-mediated DNA strand scission at AP sites. We intended to characterize the formation time course of DPC_{in} and DPC_{cl} using 2CS variants with and without a Glu residue. DPC_{in} denotes DNA-protein cross-links (DPCs) with the intact DNA oligomer; DPC_{cl} denotes DPCs with a cleaved DNA oligomer. To quantify DPC_{in} and DPC_{cl}, we optimized the protease digestion procedures and separated two types of DPCs using denaturing PAGE (Fig. S6). Using pronase E, which contains a mixture of proteolytic enzymes from *Streptomyces griseus*, we were able to separate DPCs based on their migration relative to the AP-DNA substrate. Peptide-DNA cross-links migrating slower than AP-DNA corresponded to DPC_{in}, and products migrating faster than AP-DNA but slower than SSB corresponded to DPC_{cl}, as shown in Figure S6. The separation of the two types of DPCs allowed us to follow the time-course formation of DPC_{in} and DPC_{cl} unambiguously.

Given the importance of K186 in TFAM-catalyzed AP-DNA cleavage, we chose to investigate the role of E187 in the reaction. We hypothesized that E187 could promote β-elimination by abstracting the α-H as a general base (directly or via a water molecule, as shown in Figure 1C), stabilizing the Schiff base, or both. To test this, we prepared the TFAM 2CS/E187A (2CSEA) variant and compared product yields and reaction rates with those from 2CS in TFAM-mediated AP-DNA scission under physiology pH and ionic strength conditions. In the presence of $NaBH_3CN$ (N reactions), DPC_{in} and DPC_{cl} were trapped due to the rapid reduction of imines under near neutral pH,[34] as observed in Figures S2B and S2C (left panels). The relative abundance of DPC_{in} and DPC_{cl} depends on the rate of β-elimination relative to the reduction of imine. As summarized in Table 1, although the total yields of DPCs (DPC_{in} and DPC_{cl}) were nearly identical in a 12-h reaction, 2CSEA resulted in a higher yield of DPC_{in} (89 % for 2CSEA vs. 76% for 2CS) and a lower yield of DPC_{cl} (11% for 2CSEA vs. 23% for 2CS), supporting a role of E187 in promoting β-elimination. The increased accumulation of DPC_{in} was evident with 2CSEA in gel electrophoretic analysis (compare the left panels of Figs. S2B and S2C). In the absence of $NaBH_3CN$ (X reactions), reactions undergo steps 1 through 3 (Fig. 1C), generating DPC_{in}, DPC_{cl}, and SSBs. With both 2CS and 2CSEA, the formation of DPC_{in} peaked at the first 10 min of the reaction (Fig. 3A), followed by conversion to DPC_{cl} and SSBs (Figs. S2B and S2C, right panels). Notably, compared to 2CS, a clear increase in the accumulation of DPC_{in} was observed in gel electrophoresis analysis with 2CSEA (Figs. S2B and S2C, right panels). The accumulation of DPC_{in} was more apparent when comparing the ratios of relative abundance of DPC_{in}/DPC_{cl} between 2CS and 2CSEA (Fig. 3A). Overall, these data demonstrate that E187 facilitates β-elimination in AP-DNA cleavage.

Further, the role of E187 in β-elimination was implicated when the rates of AP-DNA disappearance (k_{dis}) and DPC formation were compared. k_{dis} is a comprehensive rate constant encompassing contribution from all steps in the reaction (Fig. 1C), whereas the rate of DPC formation reflects the kinetics of several sub-steps. In the presence of $NaBH_3CN$, $k_{dis,N}$ is contributed primarily by steps 1 and 4 and, to a lesser extent, by steps 2, 3, and 5. As shown in Table 1 and Figure S3, 2CS yielded a $k_{dis,N}$ of 23 ± 2.3 (x 10^{-5} s^{-1}), and 2CSEA yielded a $k_{dis,N}$ of 44 ± 2.2 (x 10^{-5} s^{-1}). Considering that β-elimination promotes the forward equilibrium, the 2-fold higher k_{dis} with 2CSEA can be partly attributed to a compromised β-elimination reaction. Because the ratio of $k_{dis,N}/k_{dis,X}$ contains contributions from steps after the Schiff base formation in the denominator, a slower β-elimination step would result in a higher $k_{dis,N}/k_{dis,X}$ ratio. Indeed, the ratios were 4.3 for 2CS and 8.6 for 2CSEA (Table 2, pH 7.4), in keeping with slower β-elimination in the absence of E187. Regarding the formation rate of DPC_{in} ($k_{f,in}$) it contains mainly kinetic contributions from steps 1 and 4. Compared to 2CS, a 2-fold faster $k_{f,in}$ was observed with 2CSEA (Table S3, 2CS and 2CSEA with AP_{17}). With both 2CS and 2CSEA, the formation rates of DPC_{in} are comparable to k_{dis}, indicating the *in situ* trapping of DPCs by $NaBH_3CN$ was efficient (Table S3, 2CS and 2CSEA with AP_{17}). DPC_{cl} was a major product in the absence of $NaBH_3CN$, whereas only a minimal level of DPC_{cl} formed in the presence of $NaBH_3CN$. Therefore, we reason that Schiff base formation is relatively slow and β-elimination is relatively fast (but slower than reductive amination). This notion is supported

by published kinetic data regarding the Schiff base formation[35] and $NaBH_3CN$-catalyzed reductive amination in aqueous solutions.[34]

To verify these observations were indeed due to specific TFAM-DNA interactions, we carried out a control experiment with a different substrate (AP_{20}, sequence shown in Fig. 1D) containing the AP lesion 3 nt away from (5′ of) that of AP_{17}. Because the AP position in AP_{20} is away from the K186/E187 cluster in TFAM-DNA complexes, it is anticipated that the catalytic effects of these residues would diminish. As shown in Table S3 and Figures S7 and S8, in the presence of $NaBH_3CN$, $k_{dis,N}$ was much lower with AP_{20} than that of AP_{17}, with both 2CS and 2CSEA, consistent with the important roles of K186 and E187 in TFAM-mediated AP-DNA cleavage. Unlike the 5- and 9-fold difference between $k_{dis,N}$ and $k_{dis,X}$ with AP_{17} and 2CS and 2CSEA, $k_{dis,N}$ and $k_{dis,X}$ obtained with AP_{20} were nearly identical with both TFAM variants. These observations reaffirm the catalytic role of the K186/E187 cluster in TFAM-mediated AP-cleavage reactions. Importantly, unlike the 2-fold greater $k_{dis,N}$ for AP_{17} with 2CSEA as compared to that of 2CS, k_{dis} values obtained with AP_{20} were comparable (2CSEA vs. 2CS, with or without $NaBH_3CN$), reinforcing the role of E187 in β-elimination. Taken together, these experiments with site-specific AP-DNA substrates and TFAM variants demonstrate the role of E187 unequivocally in promoting the β-elimination step of the TFAM-assisted AP-lyase reaction.

AP-DNA cleavage under different pH conditions

Considering that pH could affect the protonation of solvent-exposed K186 and E187, as well as the Schiff base intermediates, we obtained reaction rates under two additional pH conditions (6.2 and 8.7) with AP_{17}. Although the physiological pH is approximately 8 in the mitochondria matrix,[36] the local pH could vary inside the nucleoid. In spite of the varying $K_{d,DNA}$ of TFAM under different pH conditions (Fig. S9C), AP_{17} was saturated by TFAM completely under the current assay conditions (4 μM of DNA and 8 μM of TFAM) based on calculations using a quadratic equation.[37] Even with the highest $K_{d,DNA}$ (~400 nM) under pH 8.7, the calculated TFAM-bound AP_{17} was greater than 92% of the total DNA in the assay. Therefore, the impact of DNA binding on the reaction rates was negligible. In terms of k_{dis} of AP_{17} (with or without $NaBH_3CN$), the rate increased with pH with both 2CS and 2CSEA (Table 2), likely due in part to the greater extent of deprotonation of key lysine residues under basic conditions, which enhances the nucleophilicity of Lys. When comparing $k_{dis,N}/k_{dis,X}$ between 2CS and 2CSEA under different pH conditions (Fig. 4A), we observed higher $k_{dis,N}/k_{dis,X}$ ratios under pH 6.2 for 2CSEA, similar to that observed at pH 7.4. However, under pH 8.7, the $k_{dis,N}/k_{dis,X}$ ratios were comparable between 2CS and 2CSEA, mainly due to the dramatic increase of $k_{dis,X}$ with both TFAM variants. The drastic increase of $k_{dis,X}$ under pH 8.7 suggest an acceleration of the rate-determining step, presumably Schiff base formation. In addition, under pH 6.2 and 7.4, 2CS and 2CSEA yielded comparable $k_{dis,X}$ values in the absence of $NaBH_3CN$ (Table 2, Fig. 4B). By contrast, under pH 8.7, a 4-fold difference in $k_{dis,X}$ was observed between 2CS and 2CSEA, indicating that other factors contributing factors may compensate for the loss of Glu (e.g., the fraction of the deprotonated Schiff base).

Because pH affects the rate of spontaneous β-elimination of AP sites (Fig. S9A and S9B), we compared the half-life of naked AP_{17} with that of TFAM-complexed AP_{17} under different pH conditions. The fold reduction in $t_{1/2}$ reflects the net effect of TFAM variants on the stability of AP sites. As shown in Table 3, $t_{1/2}$ of AP sites in free DNA decreased at higher pH conditions, consistent with faster β-elimination under basic environments. When AP_{17} was complexed with TFAM, $t_{1/2}$ was reduced by 2 orders of magnitude, with the highest fold reduction (173-fold) at pH 8.7 and approximately 100-fold at pH 6.2 and 7.4. Although the spontaneous β-elimination occurs faster under basic pH, the 173-fold reduction in $t_{1/2}$ of AP argues for a catalytic effect of TFAM. The faster reaction under basic pH could arise from an increase in the fraction of deprotonated Lys side chains.

Regarding the overall DPC yields and the relative abundance of DPC_{in} and DPC_{cl}, product profiles under pH 6.2 were comparable to those under pH 7.4 (Table 4). Under pH 8.7, a number of differences were observed. First, in the presence of $NaBH_3CN$, a significant increase in the yield of DPC_{cl} was observed, compared to those observed under pH 7.4 or 6.2. Under this condition, 2CSEA led to an increase in the DPC_{in} and a decrease in the yield of DPC_{cl}. Second, in the absence of $NaBH_3CN$, compared to 2CS, a dramatic increase in the yield of DPC_{cl} was observed. This is in contrast to the basal level of DPC_{cl} produced without $NaBH_3CN$ in the case of both 2CS and 2CSEA under pH 6.4 or pH 7.4. The yields of DPC_{cl} were 56% for 2CS vs. 29% for 2CSEA, in keeping with the role of E187 in β-elimination. The overall faster reaction under pH 8.7 could be partly owing to faster Schiff base formation due to an increased amount of deprotonated form of Lys under pH 8.7. Assuming the pKa of the solvent-exposed Lys is near 10, shifting pH from 7.4 to 8.7 would increase the fraction of the deprotonated Lys side chains by approximately 100-fold. On the other hand, E187 likely remained predominantly in the deprotonated form, and had not a significant impact on the reaction rates under the current conditions. Overall, the difference in kinetic parameters and product profiles under different pH conditions support the importance of Lys residues in these reactions.

Kinetic simulations support the role of E187 in β-elimination

To compare the rate constants of the β-elimination step between 2CS and 2CSEA directly, we fit data under three pH conditions to a simplified kinetic model using KinTek Explorer software.[38] Kinetic simulations have been shown to be useful in extracting individual rate constants, which would otherwise be difficult to isolate experimentally.[37-39] Because of the lack of data to constrain the noncovalent binding and dissociation of TFAM-DNA complexes, these steps were embedded in the Schiff base formation (Fig. 5A, step 1) and the dissociation from DPC_{cl} (Fig. 5A, step 6). On the basis of the reported on-rate of TFAM-DNA interactions, the rate of step 1 should not be limited by noncovalent binding or sliding.[40] The simplified kinetic model of reactions in the presence of $NaBH_3CN$ is shown in Figure 5A. The kinetic model in the absence of $NaBH_3CN$ is the same as that in Figure 5A, except without steps 8 and 9. Global data fitting demonstrates that the proposed kinetic model correlates largely with our experimental data (Fig. 5B and Fig. S10). As summarized in Table 5 and Table S6, although not all the rate constants were well constrained due to the lack of data to define all the sub-steps, kinetic parameters of several key steps were well defined, i.e., steps 1, 4 and 6 (Fig. 5A). Overall, the Schiff base formation was rate-limiting

for both 2CS and 2CSEA, supporting our earlier conclusion. In the presence of $NaBH_3CN$, β-elimination occurred faster than the Schiff base formation with a rate constant comparable to that of the reverse rate of step 1 (Table 5). In the absence of $NaBH_3CN$, the reverse rate constants of Schiff base formation and β-elimination were extremely small, indicating that the forward reactions of both steps were favored. Although the reverse rate constants of β-elimination were greater in the presence of $NaBH_3CN$, the rapid reduction by $NaBH_3CN$ offset the effect and drove the equilibrium forward, as evidenced by a k_6 (8500 – 9600 h^{-1}) that is 2-orders of magnitude higher than k_{-4} (58 – 59 h^{-1}).

Importantly, the rate constants of β-elimination for 2CSEA are several folds lower than that of 2CS (4-fold with $NaBH_3CN$ and 2-fold without $NaBH_3CN$) based on their best-fit values, supporting the role of E187 in β-elimination. Further, we carried out confidence contour analysis to estimate the errors associated with simulations and to reveal complex relationships between the simulated parameters [41]. The resulting confidence contours showed that the simulated rate constants were well constrained by the data in general, especially for steps 1, 4 and 6 (see lower and upper bounds in Table 5 and Table S6). With or without $NaBH_3CN$, the range of simulated data for β-elimination with 2CS is greater than that of 2CSEA (compare lower and upper bounds in Table 5), affirming a faster β-elimination with 2CS. Overall, kinetic simulations allowed the direct comparison of rate constants with 2CS and 2CSEA. The data support the role of E187 in facilitating β-elimination and demonstrate that Schiff base formation is rate-limiting in TFAM-mediated AP lyase reactions.

Conformational dynamics of the AP sites and E187 in TFAM-DNA complexes

The dynamic conformations of AP sites in duplex DNA and protein-bound complexes have been well documented by web-lab approaches[42, 43] and MD simulations.[44] The AP lesion can adopt an intrahelical or extrahelical conformation, depending on the local sequence, its complementary nucleobase, and the associated protein (see [43] and references therein). To probe the conformational dynamics of AP sites in TFAM-DNA complexes for steps 1 and 2 of the proposed mechanism (Fig. 1C), we carried out MD simulations using modified models based on the TFAM-DNA co-crystal structure (PDB: 3TQ6).[45] We built the AP lesion in AP_{17} as a closed 5-membered sugar ring based on its favored closed ring structure. We started the MD simulations with the AP lesion in its intrahelical conformation (Fig. 6A). The motion of the AP lesion was evident in the output trajectory (Fig. S11A). Although the intrahelical conformation of the AP site was maintained for the first 90 ns of 200 ns simulations, an extrahelical conformation was adopted for the remaining time (approximately 55% of the time). The rotation of the AP lesion outside the duplex structure likely facilitates the Schiff base formation by shortening the distance between the carbonyl group and the ε-amino group of K186 with a few occasions that the distance was as short as approximately 4.0 Å (Fig. S11B). L182, one of the two intercalating residues (the other being L58) in TFAM-DNA complexes [45], maintained its position in the complex (data not shown), which may help stabilize the conformation with the moiety rotated outside the helical structure. Therefore, our results demonstrate that the AP site maintains its dynamic characteristics in TFAM-DNA complexes and the transition to the extrahelical conformation likely facilitates the Schiff base formation.

To explore the interactions between E187 and the Schiff base, we built a model containing the covalently linked Schiff base intermediate formed between the C1′ atom of the AP lesion and the ε-N atom of K186 using a frame from a previous trajectory when the AP ring is proximal to K186. We carried out MD simulations using this system and observed the conformational flexibility of E187 and the Schiff base intermediate. The side chain of E187 was very flexible and observed to move towards the intermediate multiple times over the trajectory (Fig. S12). The farthest distance between the proximal O atom of the E187 side chain and the C1′ hydrogen was approximately 15.2 Å (Fig. 6B), and the closest distance was 6.9 Å (Fig. 6B). Such distances were too far for direct hydrogen abstraction by the carboxylate group to occur, it is likely that the reaction is mediated by a water molecule as proposed in Figure 1C. Together, data from MD simulations support the proposed mechanism and provide important insights into the conformational flexibility of AP sites and E187 in TFAM-DNA complexes.

DISCUSSION

Critical to the repair of ubiquitous AP sites or other nucleobase modifications are the enzymes with AP-lyase activities. AP endonucleases are best-studied enzymes specific to AP sites, incising the DNA backbone at the 5′-side of the deoxyribose group and leaving a 5′-deoxyribose phosphate (dRp) moiety on one of the cleaved strands.[46] AP endonucleases function with monofunctional glycosylases in base excision repair (BER).[47] Equally important are bifunctional DNA glycosylases with both DNA glycosylase and AP-lyase activities. These enzymes catalyze the β-elimination reaction of AP sites upon the enzymatic cleavage of damaged nucleobases.[47] Importantly, the AP-lyase activity is not limited to these well-studied enzymes. A body of work by the Greenberg and Gates laboratories has shown that free amino groups in DNA-binding proteins and nucleobases can catalyze similar reactions.[48-51] For example, Greenberg and associates have demonstrated that Lys residues of histone tails can promote strand scission at AP sites in reconstituted nucleosome particles.[48, 49] Gates and associates have shown that *in vitro* amino groups of the nucleoside 3′ or 5′ of the nucleoside opposing the AP lesion can catalyze similar reactions in duplex DNA substrates with a variety of DNA sequence contexts, and that biological amines, such as spermine, can accelerate the reaction.[50-53]

Similarly, we have demonstrated that, *in vitro* and *in cellulo*, TFAM, a key DNA-packaging factor in mitochondria, promotes AP-DNA scission via Schiff base chemistry.[20, 21] The activity differs from the APE1-catalyzed AP-DNA cleavage and likely complement APE1 repair given the high abundance of TFAM. Besides, the TFAM-mediated cleavage also forms TFAM-DPCs involving Cys residues (Michael-type adduct) and Lys residues (Schiff base).[21] Given the heterogeneous characteristics of TFAM-DPCs, we prepared the Cys-null variant of TFAM to probe the role of key Lys and Glu residues and the properties of resulting DPCs without interference from Cys-derived DPCs. Our kinetic and mass spectrometric analyses demonstrate that, compared to wt TFAM, 2CS maintains similar interactions with AP-DNA and is a suitable variant for our experimental purposes. Besides, mass spectrometry data revealed additional Lys residues (e.g., K111) that can participate in the reaction after the AP lesion reacts reversibly with K186. By contrast, wt TFAM cross-links with AP-DNA primarily at C49. Stability analysis of 2CS-derived DPCs allowed

comparison with other imine-based DPCs directly. 2CS-DPCs have a $t_{1/2}$ of 7 h under physiological conditions, comparable to a $t_{1/2}$ of 10-14 h of AP-DNA-peptide cross-links derived from histone H2 and H4 proteins,[54] and much more stable than 5-formylcytosine-histone DPC ($t_{1/2}$ = ~1.8 h)[55] and 5-formyluracil-histone DPC ($t_{1/2}$ = ~28 min).[56] By contrast, wt TFAM-DPCs formed predominantly via Michael-additions have a $t_{1/2}$ of 43 h, even more stable than histone-DPCs. The biological significance of the relatively stable TFAM-DCPs warrants further investigation.

Intriguingly, TFAM has a higher abundance of Glu compared to its average abundance in the human proteome. In addition, more than half of the Glu residues are clustered with Lys residues in TFAM, making them prime candidates as a general base for H-abstraction at the C2′ carbon directly or via a water molecule, or acting as a counterion of the protonated Schiff base. These roles of carboxylate side chains have been documented for key residues in bifunctional glycosylases and other DNA repair enzymes. For example, E23 of T4 endonuclease V stabilizes the Schiff base intermediate and also potentially participates in β-elimination.[27] T4 endonuclease V is a bifunctional glycosylase from bacteriophage T4 that removes the pyrimidine dimer DNA adduct. On the other hand, histone H2B and H4 tails catalyze AP-lyase reactions despite the lack of Glu, Asp, and His residues, which results in a rate-limiting β-elimination step.[57] The introduction of Glu, Asp, and His proximal to key Lys residues increases the overall rate of the AP-DNA scission.[57] On the contrary, the high abundance of Glu in TFAM likely results in a fast β-elimination step, rendering Schiff base formation rate-limiting. Although further studies are needed to clarify the effects of other Glu on the aforementioned steps, our data demonstrate unambiguously that E187 facilitates β-elimination with defined AP-DNA substrates.

Aside from the amino acid compositions of TFAM, the dynamics of AP lesions contribute to the kinetics of the AP-lyase reaction. On the basis of MD simulation data, the extrahelical conformations were observed in the second half of the trajectory, suggesting that the conformational change may partially limit the Schiff base formation. The extrahelical conformation of AP sites has been observed in co-crystal structures of several other repair enzymes, including uracil-DNA glycosylase,[58] alkylated-base glycosylase AlkA,[59] and APE1.[60] The conformational flexibility of AP sites may be enhanced by L182, one of the two intercalating residues (the other being L58) in TFAM-DNA complexes. These intercalating residues play a major role in facilitating a U-turn DNA structure for transcription initiation and DNA compaction.[45] L182 may promote the conformational flexibilities of the AP lesion by stabilizing the local duplex DNA structure, analogous to DNA-intercalating residues in other base-flipping glycosylases.[61, 62] In addition, the conformational flexibility of the E187 side chain may facilitate the reaction by shortening the distance between E187 and the C2′ position.

mtDNA is turned over rapidly compared to nuclear DNA, with a reported half-life in a matter of days.[13] Recently, mtDNA degradation has also emerged as an important DNA damage response mechanism.[2, 4, 7, 8]. The induction of AP sites in mitochondria leads to a rapid decline in mtDNA copy number without increasing the mutation load.[63] The high abundance of Lys and Glu residues in TFAM supports the role of TFAM in facilitating strand scission at ubiquitous AP sites. Although the observed rate of AP-DNA cleavage is

much slower than other DNA repair enzymes, the abundance of TFAM in nucleoids and our detection of elevated TFAM-DPCs upon inducing mitochondrial AP sites in HeLa and HEK293 cells[21, 22] argue the involvement TFAM in processing AP sites in mitochondria. The strand scission at AP sites converts AP lesions to more deleterious “roadblocks” in the forms of DPCs and SSBs to various mtDNA transactions, which could potentially serve as signals for recruiting additional factors (e.g., DNA nucleases) or for purifying selection against damaged mtDNA molecules. The rapid AP-DNA degradation supports the disposable characteristic of mtDNA[7] and a proposed role of mtDNA as a cellular genotoxic stress sentinel.[3]

In sum, we have demonstrated the role of E187 in facilitating β-elimination during TFAM-mediated AP-lyase reactions. Although E187 is a representative residue proximal to a key Lys (K186), the abundance of Glu in TFAM and the large fraction of Glu clustered with Lys suggest a general role of Glu in facilitating AP-lyase reactions. Unlike specific Glu located in the enzyme active site, the extent of contribution of different Glu residues likely varies based on the local interactions and the conformational dynamics of the AP lesion in a given sequence context in TFAM-DNA complexes.

MATERIALS AND METHODS

Reagents

Unless specified otherwise, chemicals were from Sigma Aldrich (St. Louis, MO) or Fisher Scientific and were of the highest grade. MS grade trypsin was from Fisher Scientific. *E. coli* BL21 (DE3) competent cells and uracil DNA glycosylase (UDG) were from New England Biolabs (Cat. No M0280S, Ipswich, MA). Pronase E was from MedChemExpress (Monmouth Junction, NJ, Cat. No HY-114158). The pET28a vectors expressing the mature form of human TFAM (amino acid 43-246) variants were constructed by GenScript (Piscataway, NJ). Human TFAM cDNA was inserted at the restriction enzyme site Nde I. Constructs expressing TFAM variants were created by site-directed mutagenesis by GenScript. Oligodeoxynucleotides were synthesized and HPLC-purified by Integrated DNA Technologies (Coralville, IA).

Electrophoretic mobility shift assay

The reaction solution contains 20 mM HEPES (pH 7.4), 90 mM NaCl, 20 mM EDTA, 4 μM DNA substrate (dU-containing duplex), and increasing concentrations TFAM. All reactions were prepared on ice and mixed with a loading buffer containing glycerol with bromophenol and xylene-cyanol. Electrophoresis was carried out on a 6% polyacrylamide (acrylamide/bis-acrylamide) gel in 0.35X TBE (Tris-Borate-EDTA) buffer at 100 V and 4 °C. The gel was imaged with a Typhoon imager (Cytiva, previously GE Healthcare Life Sciences) and quantified using ImageQuant software (Cytiva). Data were graphed using GraphPad Prism (v8.0).

Reactions of TFAM with AP-DNA

TFAM and AP-DNA reactions were conducted and analyzed similarly to the previous procedures with modifications [20]. Briefly, wild-type (wt) TFAM or variants were incubated

with AP-DNA to monitor the rates of strand scission and SSB and DPC formation. Reactions contained 4 μM AP-DNA, 8 μM TFAM (wt or variant), 20 mM HEPES (pH 7.4), 90 mM NaCl, and 20 mM EDTA, with or without 25 mM $NaBH_3CN$. Reactions under pH 6.2 were in 50 mM of MES (2-(*N*-morpholino)ethanesulfonic acid) buffer, and reactions under pH 8.7 were in 50 mM sodium carbonate-bicarbonate buffer. Reactions were carried out at 37 °C with aliquots taken at varying times and quenched by adding an equal volume of 0.2 M $NaBH_4$, followed by rapid cooling on ice. Samples were stored at −80 °C until electrophoretic analysis. To analyze the DPCs without enzymatic digestion, SDS-urea polyacrylamide gel electrophoresis (PAGE) was used. Samples were mixed with a gel-loading solution containing 95 % (v/v) formamide, 50 mM EDTA and 1% SDS, and analyzed on an 8 cm × 10 cm SDS-urea (7 M) PAGE (4% -16%). To analyze the DPCs by denaturing PAGE, DPCs were digested with pronase E (0.5 mg/mL, 41 °C overnight), followed by mixing with a 1.5-volume of loading solution containing 95 % (v/v) formamide and 50 mM EDTA for electrophoresis (16% polyacrylamide/bis-acrylamide (19:1), 7 M urea, 38 cm × 30 cm). Gel images were acquired and analyzed as described above. The apparent DNA disappearance rate was obtained by fitting the percent yield of intact DNA to a single-exponential function as described [20]. Percent yields of DPCs and SSBs were fitted to a one-phase decay single-exponential function with 100% set as the initial value.

Thermostability and half-life of TFAM-DPCs

The stability and half-life of DPCs under different temperatures were examined by incubating DPC products resulting from a 15-h reaction of TFAM and AP-DNA under pH 7.4 in the absence of $NaBH_3CN$. The reaction products were then incubated in a dry bath incubator for 1 h under varying temperatures (40°C, 61°C, 66°C, 76°C, 85°C) and quenched with 0.1 M $NaBH_4$. Control reactions were quenched with $NaBH_4$ before heating. The resulting products were quantified without protease digestion by using a gradient (4%-16%) SDS-urea-PAGE gel (7.5 ×10 cm). The half-life of TFAM DPCs was analyzed by incubating the reaction products at 37 °C with an aliquot taken at varying times for SDS-urea-PAGE analysis. The percent yields of DPCs (based on intensity ratios of DPCs/(DPCs+SSBs)) over time were fit to a one-phase decay single-exponential to obtain the half-life.

Half-life of AP-DNA

Without TFAM, 4 μM of AP-DNA was incubated in 20 mM HEPES (pH 7.4), 90 mM NaCl, and 20 mM EDTA under 37 °C for varying times. Reaction aliquots were quenched with an equal volume of 0.2 M $NaBH_4$, followed by rapid cooling on ice. Samples were stored at −80 °C until electrophoretic analysis.

Identification of cross-linking amino acid residues in TFAM DPCs by mass spectrometry

TFAM and AP-DNA reaction products after a 24-h reaction were digested by trypsin in 100 mM Tris-HCl pH 8.0 and 20 mM $CaCl_2$ at 37°C for 12 to 14 h. Samples were purified and analyzed by tandem mass spectrometry according to published procedures [21].

Kinetic simulations

Data from TFAM-mediated AP-DNA cleavage reactions under pH 6.2, 7.4 and 8.7 were fit globally into a multi-step kinetic model (Fig. 5A) using KinTek Explorer 7 [38]. The imported data were concentrations of products (remaining AP-DNA, DPC_{in}, DPC_{cl}, and SSBs) as a function of the reaction time. Initial reactant concentrations were 4 μM for DNA (D+DH in Fig. 5A) and 8 μM for TFAM in a 12-h reaction. The observed SSB concentration was defined as the sum of SSB and the SSBH (Fig. 5A). Individual rate constants were allowed to fluctuate. FitSpace [41] calculation was used to determine the reliability of the fit, and the lower and upper bounds were obtained by setting the threshold at bound as 0.95. FitSpace confidence contours analysis was used to evaluate whether the simulated data were unique and well-constrained. FitSpace results were computed for 0.6 Chi^2 threshold limit. The boundary of kinetic parameters was calculated when the Chi^2 threshold was set as 0.95.

MD simulations

Conventional MD simulations (200 ns) were carried out with two systems of TFAM-DNA complexes with a ring-closed AP site or a Schiff base intermediate. The 3D coordinates of TFAM-DNA complexes were obtained from the crystal structure of PDB ID 3TQ6 [45]. XLeap editor was used to remove the nucleobase at the AP_{17} lesion position, build a covalent bond between the lesion and lysine, modify partial charges and generate input files for MD simulations. MD simulations were performed using the Amber18 package with GPU implementation [64]. The protein was parameterized by using Amber Force Field FF14SB and DNA by AMBER bsc1 [64-66]. Antechamber was used to calculate the partial charge of the Schiff base intermediate in the system using General Amber Force Field (GAFF) [67]. Both systems were minimized in three steps, hydrogen, side chains, and the entire system. The systems were explicitly solvated using TIP3P water model in a rectangular box of periodic boundaries at 12 Å from any atom and 27 positive counter ions (Na^+) were added to neutralize the overall system charge.

The solvated systems were then minimized, followed by isothermic-isobaric (NPT) ensemble equilibration in 25 K increments from 50 to 298 K, first for water only and then for the entire system, for 200 ps at each temperature. MD trajectories were from over 200 ns at a 1-ps interval with a 2-fs timestep under constant pressure and temperature. Particle mesh Ewald [68] and the SHAKE algorithm [69] were applied for long-range electrostatics and fixed heavy atom–hydrogen bond lengths. The trajectory output files were processed with PTRAJ to contain 20,000 frames after stripping water molecules and ions, each representing a 0.01-ns timestep [70]. Each trajectory was aligned using the backbone of the first frame and analyzed by using Visual Molecular Dynamics (VMD) [71] and PyMOL [72].

Supplementary Material

Refer to Web version on PubMed Central for supplementary material.

Acknowledgments

We thank Dr. Laurie S. Kaguni for helpful discussions.

Funding

This work was supported by National Institutes of Health (NIH) grant R35 GM128854 (to L.Z.), National Science Foundation grant MCB-1932984 (to C.C.), and the University of California, Riverside.

REFERENCES

1. Friedman JR, and Nunnari J (2014) Mitochondrial form and function, Nature 505, 335. [PubMed: 24429632]
2. Alexeyev M, Shokolenko I, Wilson G, and LeDoux S (2013) The maintenance of mitochondrial DNA integrity—critical analysis and update, Cold Spring Harb. Perspect. Biol 5, a012641. [PubMed: 23637283]
3. Wu Z, Sainz AG, and Shadel GS (2021) Mitochondrial DNA: cellular genotoxic stress sentinel, Trends in Biochemical Sciences 46, 812–821. [PubMed: 34088564]
4. Zhao L, and Sumberaz P (2020) Mitochondrial DNA Damage: Prevalence, Biological Consequence, and Emerging Pathways, Chem. Res. Toxicol 33, 2491–2502. [PubMed: 32486637]
5. Young MJ, and Copeland WC (2016) Human mitochondrial DNA replication machinery and disease, Curr. Opin. Genet. Dev 38, 52–62. [PubMed: 27065468]
6. Gustafson MA, Sullivan ED, and Copeland WC (2020) Consequences of compromised mitochondrial genome integrity, DNA Repair 93, 102916. [PubMed: 33087282]
7. Shokolenko IN, and Alexeyev MF (2015) Mitochondrial DNA: A disposable genome?, Biochim. Biophys. Acta, Mol. Basis Dis 1852, 1805–1809.
8. Zhao L (2019) Chapter Ten - Mitochondrial DNA degradation: A quality control measure for mitochondrial genome maintenance and stress response, In The Enzymes (Zhao L, and Kaguni LS, Eds.), pp 311–341, Academic Press.
9. Scheibye-Knudsen M, Fang EF, Croteau DL, Wilson DM, and Bohr VA (2015) Protecting the mitochondrial powerhouse, Trends in cell biology 25, 158–170. [PubMed: 25499735]
10. Kauppila TE, Kauppila JH, and Larsson N-G (2017) Mammalian mitochondria and aging: an update, Cell Metab. 25, 57–71. [PubMed: 28094012]
11. Valente WJ, Ericson NG, Long AS, White PA, Marchetti F, and Bielas JH (2016) Mitochondrial DNA exhibits resistance to induced point and deletion mutations, Nucleic acids research 44, 8513–8524. [PubMed: 27550180]
12. Leuthner TC, Benzing L, Kohrn BF, Bergemann CM, Hipp MJ, Hershberger KA, Mello DF, Sokolskyi T, Stevenson K, and Merutka IR (2022) Resistance of mitochondrial DNA to cadmium and Aflatoxin B1 damage-induced germline mutation accumulation in C. elegans, Nucleic Acids Research 50, 8626–8642. [PubMed: 35947695]
13. Gross NJ, Getz GS, and Rabinowitz M (1969) Apparent turnover of mitochondrial deoxyribonucleic acid and mitochondrial phospholipids in the tissues of the rat, J. Biol. Chem 244, 1552–1562. [PubMed: 5773057]
14. West AP, Khoury-Hanold W, Staron M, Tal MC, Pineda CM, Lang SM, Bestwick M, Duguay BA, Raimundo N, MacDuff DA, Kaech SM, Smiley JR, Means RE, Iwasaki A, and Shadel GS (2015) Mitochondrial DNA stress primes the antiviral innate immune response, Nature 520, 553–557. [PubMed: 25642965]
15. Xian H, Watari K, Sanchez-Lopez E, Offenberger J, Onyuru J, Sampath H, Ying W, Hoffman HM, Shadel GS, and Karin M (2022) Oxidized DNA fragments exit mitochondria via mPTP-and VDAC-dependent channels to activate NLRP3 inflammasome and interferon signaling, Immunity 55, 1370–1385. e1378. [PubMed: 35835107]
16. Peeva V, Blei D, Trombly G, Corsi S, Szukszto MJ, Rebelo-Guiomar P, Gammage PA, Kudin AP, Becker C, and Altmüller J (2018) Linear mitochondrial DNA is rapidly degraded by components of the replication machinery, Nat. Commun 9, 1727. [PubMed: 29712893]
17. Nissanka N, Bacman SR, Plastini MJ, and Moraes CT (2018) The mitochondrial DNA polymerase gamma degrades linear DNA fragments precluding the formation of deletions, Nat. Commun 9, 2491. [PubMed: 29950568]
18. Matic S, Jiang M, Nicholls TJ, Uhler JP, Dirksen-Schwanenland C, Polosa PL, Simard M-L, Li X, Atanassov I, and Rackham O (2018) Mice lacking the mitochondrial exonuclease MGME1

accumulate mtDNA deletions without developing progeria, Nat. Commun 9, 1202. [PubMed: 29572490]

19. Milenkovic D, Sanz-Moreno A, Calzada-Wack J, Rathkolb B, Veronica Amarie O, Gerlini R, Aguilar-Pimentel A, Misic J, Simard M-L, and Wolf E (2022) Mice lacking the mitochondrial exonuclease MGME1 develop inflammatory kidney disease with glomerular dysfunction, PLoS Genet. 18, e1010190. [PubMed: 35533204]
20. Xu W, Boyd RM, Tree MO, Samkari F, and Zhao L (2019) Mitochondrial transcription factor A promotes DNA strand cleavage at abasic sites, Proc. Natl. Acad. Sci. U. S. A 116, 17792–17799. [PubMed: 31413200]
21. Xu W, Tang J, and Zhao L (2023) DNA-Protein Cross-Links Between Abasic DNA Damage and Mitochondrial Transcription Factor A (TFAM), Nucleic Acids Research 51, 41–53. [PubMed: 36583367]
22. Xu W, and Zhao L (2022) An enzyme-linked immunosorbent assay for the detection of mitochondrial DNA-protein cross-links from mammalian cells, DNA 2, 264–278.
23. Kaufman BA, Durisic N, Mativetsky JM, Costantino S, Hancock MA, Grutter P, and Shoubridge EA (2007) The mitochondrial transcription factor TFAM coordinates the assembly of multiple DNA molecules into nucleoid-like structures, Mol. Biol. Cell 18, 3225–3236. [PubMed: 17581862]
24. Hillen HS, Morozov YI, Sarfallah A, Temiakov D, and Cramer P (2017) Structural basis of mitochondrial transcription initiation, Cell 171, 1072–1081. e1010. [PubMed: 29149603]
25. Zamudio-Ochoa A, Morozov YI, Sarfallah A, Anikin M, and Temiakov D (2022) Mechanisms of mitochondrial promoter recognition in humans and other mammalian species, Nucleic Acids Research 50, 2765–2781. [PubMed: 35191499]
26. Swenberg JA, Lu K, Moeller BC, Gao LN, Upton PB, Nakamura J, and Starr TB (2011) Endogenous versus exogenous DNA adducts: their role in carcinogenesis, epidemiology, and risk assessment, Toxicological Sciences 120, S130–S145. [PubMed: 21163908]
27. Manuel RC, Latham KA, Dodson M, and Lloyd RS (1995) Involvement of Glutamic Acid 23 in the Catalytic Mechanism of T4 Endonuclease V (*), J. Biol. Chem 270, 2652–2661. [PubMed: 7852333]
28. Vik ES, Alseth I, Forsbring M, Helle IH, Morland I, Luna L, Bjørås M, and Dalhus B (2012) Biochemical mapping of human NEIL1 DNA glycosylase and AP lyase activities, DNA Repair 11, 766–773. [PubMed: 22858590]
29. Lloyd RS (2022) Complex Roles of NEIL1 and OGG1: Insights Gained from Murine Knockouts and Human Polymorphic Variants, DNA 2, 279–301.
30. Kumar A, Reed AJ, Zahurancik WJ, Daskalova SM, Hecht SM, and Suo Z (2022) Interlocking activities of DNA polymerase β in the base excision repair pathway, Proc. Natl. Acad. Sci. U. S. A 119, e2118940119. [PubMed: 35238634]
31. Sakmar TP, Franke RR, and Khorana HG (1989) Glutamic acid-113 serves as the retinylidene Schiff base counterion in bovine rhodopsin, Proc. Natl. Acad. Sci. U. S. A 86, 8309–8313. [PubMed: 2573063]
32. Tang J, Zhao W, Hendricks NG, and Zhao L (2021) High-Resolution Mapping of Amino Acid Residues in DNA–Protein Cross-Links Enabled by Ribonucleotide-Containing DNA, Analytical Chemistry 93, 13398–13406. [PubMed: 34559515]
33. Cuppari A, Fernández-Millán P, Battistini F, Tarrés-Solé A, Lyonnais S, Iruela G, Ruiz-Lopez E, Enciso Y, Rubio-Cosials A, and Prohens R (2019) DNA specificities modulate the binding of human transcription factor A to mitochondrial DNA control region, Nucleic acids research 47, 6519–6537. [PubMed: 31114891]
34. Borch RF, Bernstein MD, and Durst HD (1971) Cyanohydridoborate anion as a selective reducing agent, Journal of the American Chemical Society 93, 2897–2904.
35. Cordes E, and Jencks W (1962) On the mechanism of Schiff base formation and hydrolysis, Journal of the American Chemical Society 84, 832–837.
36. Casey JR, Grinstein S, and Orlowski J (2010) Sensors and regulators of intracellular pH, Nat. Rev. Mol. Cell Biol 11, 50–61. [PubMed: 19997129]

37. Xu W, Zhao W, Morehouse N, Tree MO, and Zhao L (2019) Divalent cations alter the rate-limiting step of PrimPol-catalyzed DNA elongation, J. Mol. Biol 431, 673–686. [PubMed: 30633872]
38. Johnson KA, Simpson ZB, and Blom T (2009) Global Kinetic Explorer: A new computer program for dynamic simulation and fitting of kinetic data, Analytical Biochemistry 387, 20–29. [PubMed: 19154726]
39. Zhao L, Pence MG, Eoff RL, Yuan S, Fercu CA, and Guengerich FP (2014) Elucidation of kinetic mechanisms of human translesion DNA polymerase κ using tryptophan mutants, FEBS J. 281, 4394–4410. [PubMed: 25065501]
40. King GA, Hashemi Shabestari M, Taris K-KH, Pandey AK, Venkatesh S, Thilagavathi J, Singh K, Krishna Koppisetti R, Temiakov D, and Roos WH (2018) Acetylation and phosphorylation of human TFAM regulate TFAM–DNA interactions via contrasting mechanisms, Nucleic acids research 46, 3633–3642. [PubMed: 29897602]
41. Johnson KA, Simpson ZB, and Blom T (2009) FitSpace Explorer: An algorithm to evaluate multidimensional parameter space in fitting kinetic data, Analytical Biochemistry 387, 30–41. [PubMed: 19168024]
42. Cuniasse P, Fazakerley G, Guschlbauer W, Kaplan B, and Sowers L (1990) The abasic site as a challenge to DNA polymerase: a nuclear magnetic resonance study of G, C and T opposite a model abasic site, J. Mol. Biol 213, 303–314. [PubMed: 2342108]
43. Rachofsky EL, Seibert E, Stivers JT, Osman R, and Ross JA (2001) Conformation and dynamics of abasic sites in DNA investigated by time-resolved fluorescence of 2-aminopurine, Biochemistry 40, 957–967. [PubMed: 11170417]
44. Bignon E, Claerbout VE, Jiang T, Morell C, Gillet N, and Dumont E (2020) Nucleosomal embedding reshapes the dynamics of abasic sites, Sci. Rep 10, 1–10. [PubMed: 31913322]
45. Rubio-Cosials A, Sydow JF, Jiménez-Menéndez N, Fernández-Millán P, Montoya J, Jacobs HT, Coll M, Bernadó P, and Solà M (2011) Human mitochondrial transcription factor A induces a U-turn structure in the light strand promoter, Nat. Struct. Mol. Biol 18, 1281–1289. [PubMed: 22037172]
46. Whitaker AM, and Freudenthal BD (2018) APE1: A skilled nucleic acid surgeon, DNA Repair 71, 93–100. [PubMed: 30170830]
47. Beard WA, Horton JK, Prasad R, and Wilson SH (2019) Eukaryotic base excision repair: new approaches shine light on mechanism, Annu. Rev. Biochem 88, 137. [PubMed: 31220977]
48. Sczepanski JT, Wong RS, McKnight JN, Bowman GD, and Greenberg MM (2010) Rapid DNA–protein cross-linking and strand scission by an abasic site in a nucleosome core particle, Proc. Natl. Acad. Sci. U. S. A 107, 22475–22480. [PubMed: 21149689]
49. Zhou C, Sczepanski JT, and Greenberg MM (2012) Mechanistic studies on histone catalyzed cleavage of apyrimidinic/apurinic sites in nucleosome core particles, Journal of the American Chemical Society 134, 16734–16741. [PubMed: 23020793]
50. Price NE, Johnson KM, Wang J, Fekry MI, Wang Y, and Gates KS (2014) Interstrand DNA–DNA cross-link formation between adenine residues and abasic sites in duplex DNA, Journal of the American Chemical Society 136, 3483–3490. [PubMed: 24506784]
51. Catalano MJ, Liu S, Andersen N, Yang Z, Johnson KM, Price NE, Wang Y, and Gates KS (2015) Chemical structure and properties of interstrand cross-links formed by reaction of guanine residues with abasic sites in duplex DNA, Journal of the American Chemical Society 137, 3933–3945. [PubMed: 25710271]
52. Amin SBM, Islam T, Price NE, Wallace A, Guo X, Gomina A, Heidari M, Johnson KM, Lewis CD, Yang Z, and Gates KS (2022) Effects of Local Sequence, Reaction Conditions, and Various Additives on the Formation and Stability of Interstrand Cross-Links Derived from the Reaction of an Abasic Site with an Adenine Residue in Duplex DNA, ACS omega 7, 36888–36901. [PubMed: 36278095]
53. Haldar T, Jha JS, Yang Z, Nel C, Housh K, Cassidy OJ, and Gates KS (2022) Unexpected complexity in the products arising from NaOH-, heat-, amine-, and glycosylase-induced strand cleavage at an abasic site in DNA, Chem. Res. Toxicol 35, 218–232. [PubMed: 35129338]

54. Wei X, Wang Z, Hinson C, and Yang K (2022) Human TDP1, APE1 and TREX1 repair 3′-DNA–peptide/protein cross-links arising from abasic sites in vitro, Nucleic acids research 50, 3638–3657. [PubMed: 35349719]
55. Ji S, Shao H, Han Q, Seiler CL, and Tretyakova NY (2017) Reversible DNA–Protein Cross-Linking at Epigenetic DNA Marks, Angew. Chem. Int. Ed 56, 14130–14134.
56. Zou G, Liu C, Zeng W, Yang W, Zhang K, Xie Y, Chen C, and Zhou X (2020) Regulable DNA–Protein interactions in vitro and vivo at epigenetic DNA marks, CCS Chemistry 2, 54–63.
57. Yang K, and Greenberg MM (2019) Histone tail sequences balance their role in genetic regulation and the need to protect DNA against destruction in nucleosome core particles containing abasic sites, ChemBioChem 20, 78–82. [PubMed: 30307690]
58. Slupphaug G, Mol CD, Kavli B, Arvai AS, Krokan HE, and Tainer JA (1996) A nucleotide-flipping mechanism from the structure of human uracil–DNA glycosylase bound to DNA, Nature 384, 87–92. [PubMed: 8900285]
59. Hollis T, Ichikawa Y, and Ellenberger T (2000) DNA bending and a flip-out mechanism for base excision by the helix–hairpin–helix DNA glycosylase, Escherichia coli AlkA, EMBO J. 19, 758–766. [PubMed: 10675345]
60. Freudenthal BD, Beard WA, Cuneo MJ, Dyrkheeva NS, and Wilson SH (2015) Capturing snapshots of APE1 processing DNA damage, Nat. Struct. Mol. Biol 22, 924. [PubMed: 26458045]
61. Stivers JT (2004) Site-specific DNA damage recognition by enzyme-induced base flipping, Progress in nucleic acid research and molecular biology, 37–65.
62. Mullins EA, Rodriguez AA, Bradley NP, and Eichman BF (2019) Emerging roles of DNA glycosylases and the base excision repair pathway, Trends in biochemical sciences 44, 765–781. [PubMed: 31078398]
63. Kozhukhar N, Spadafora D, Fayzulin R, Shokolenko IN, and Alexeyev M (2016) The efficiency of the translesion synthesis across abasic sites by mitochondrial DNA polymerase is low in mitochondria of 3T3 cells, Mitochondrial DNA Part A 27, 4390–4396.
64. Case D, Ben-Shalom I, Brozell S, Cerutti D, Cheatham T III, Cruzeiro V, Darden T, Duke R, Ghoreishi D, and Gilson M (2018) AMBER 2018; 2018, University of California, San Francisco.
65. Maier JA, Martinez C, Kasavajhala K, Wickstrom L, Hauser KE, and Simmerling C (2015) ff14SB: improving the accuracy of protein side chain and backbone parameters from ff99SB, J. Chem. Theory Comput 11, 3696–3713. [PubMed: 26574453]
66. Ivani I, Dans PD, Noy A, Pérez A, Faustino I, Hospital A, Walther J, Andrio P, Goñi R, and Balaceanu A (2016) Parmbsc1: a refined force field for DNA simulations, Nat. Methods 13, 55–58. [PubMed: 26569599]
67. Wang J, Wolf RM, Caldwell JW, Kollman PA, and Case DA (2004) Development and testing of a general amber force field, J. Comput. Chem 25, 1157–1174. [PubMed: 15116359]
68. Sagui C, Pedersen LG, and Darden TA (2004) Towards an accurate representation of electrostatics in classical force fields: Efficient implementation of multipolar interactions in biomolecular simulations, Journal of chemical physics 120, 73–87. [PubMed: 15267263]
69. Ryckaert J-P, Ciccotti G, and Berendsen HJ (1977) Numerical integration of the cartesian equations of motion of a system with constraints: molecular dynamics of n-alkanes, J. Chem. Phys 23, 327–341.
70. Roe DR, and Cheatham TE III (2013) PTRAJ and CPPTRAJ: software for processing and analysis of molecular dynamics trajectory data, J. Chem. Theory Comput 9, 3084–3095. [PubMed: 26583988]
71. Humphrey W, Dalke A, and Schulten K (1996) VMD: visual molecular dynamics, Journal of molecular graphics 14, 33–38. [PubMed: 8744570]
72. DeLano WL (2002) The PyMOL Molecular Graphics System DeLano Scientific, San Carlos, CA, USA.

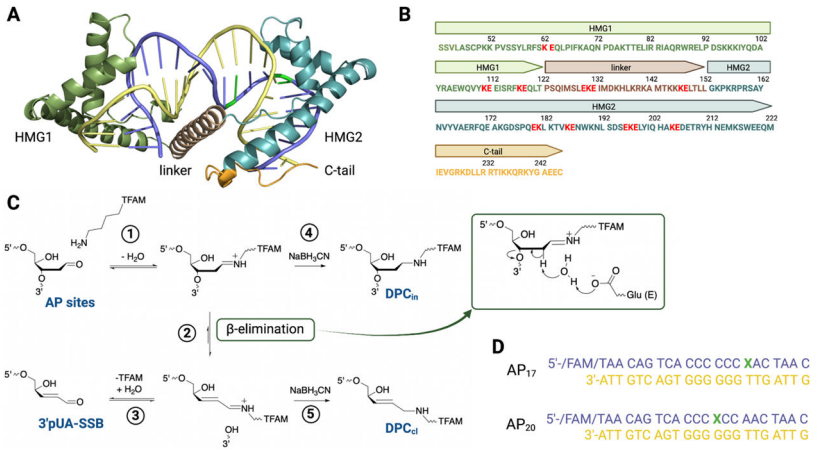

Figure 1.

Structural basis and proposed mechanism of TFAM-facilitated AP-DNA strand scission. (**A**) The crystal structure of TFAM (PDB:3TQ6) complexed with a DNA duplex substrate containing the light-strand promoter (LSP) sequence. Two high-mobility group (HMG) domains are in green (HMG1) and cyan (HMG2); the linker region is in light pink; the C-terminal tail is in yellow; two abasic site positions are in green (DNA sequences in D). (**B**) The primary sequence of TFAM with Glu-Lys clusters is highlighted in red. (**C**) Proposed mechanisms of TFAM-facilitated AP-DNA strand scission and the role of Glu acting as a general base to abstract the α-proton of the Schiff base in the β-elimination step (an optional water molecule is included). Alternately, Glu can also serve as a counter ion to stabilize the Schiff base (not shown). Major products are labeled in blue. DPC_{in} denotes DNA-protein cross-links (DPCs) with the intact DNA oligomer; DPC_{cl} denotes DPCs with a cleaved DNA oligomer; 3′pUA-SSB denotes the DNA single-strand break product with 3′-phospho-α,β-unsaturated aldehyde residue. (**D**) AP-DNA substrates (AP_{17} and AP_{20}) containing a site-specific modification. X indicates an AP lesion, converted from a deoxyuridine (dU) precursor using UDG.

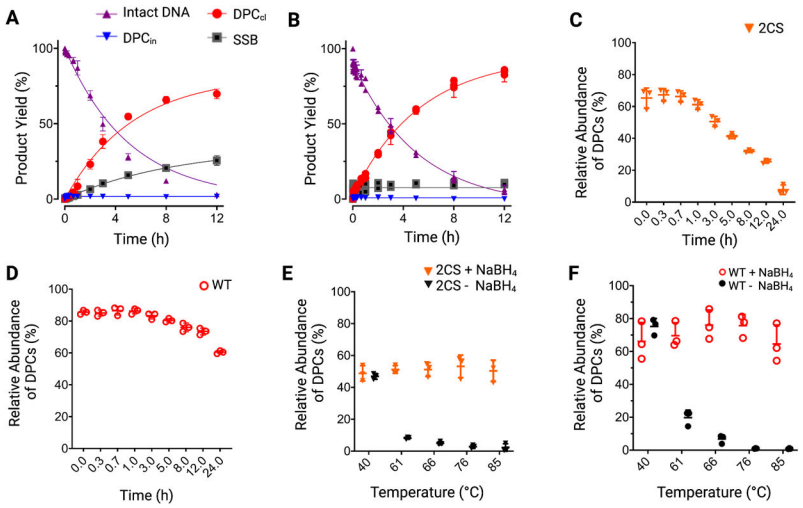

Figure 2.

Comparison of wt TFAM and 2CS in AP-DNA cleavage reactions and the stability of the resulting DPCs. Quantification of AP-DNA, DPC, and SSB in TFAM-mediated AP-DNA strand scission reactions with (**A**) 2CS and (**B**) wt TFAM. Representative gel images are shown in Fig. S2. The stability of TFAM-DPCs with (**C**) 2CS and (**D**) wt TFAM. Fitting the change of relative abundance of DPCs with time to a single exponential decay equation resulted in a half-life of 7 h for 2CS and 43 h for wt TFAM. The relative abundance is calculated based on the intensities of DPCs divided by the sum of the intensities of DPCs and SSBs. The thermostability of DPCs formed in reactions with (**E**) 2CS or (**F**) wt TFAM. DPCs used in (C) through (F) were from a 15-h reaction with TFAM and AP-DNA without $NaBH_3CN$. Representative gel images are shown in Fig. S4.

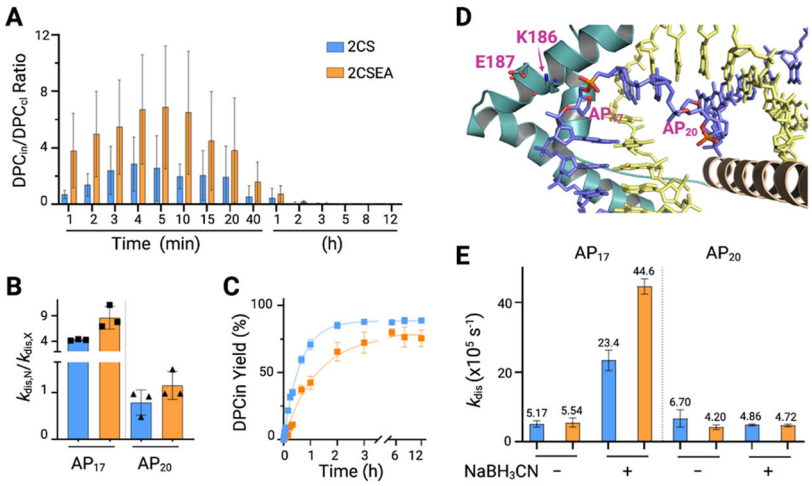

Figure 3.

Involvement of E187 in β-elimination demonstrated using reactions of TFAM variants (blue for 2CS and orange for 2CSEA) with different AP-DNA substrates (AP_{17} and AP_{20}). (**A**) Instantaneous ratios of the yield of DPCs (DPC_{in}/DPC_{cl}) in a 12-h reaction without $NaBH_3CN$. The accumulation of DPC_{in} was apparent within 1 h for 2CSEA. (**B**) Ratios of the rate of AP-DNA disappearance in the presence of $NaBH_3CN$ ($k_{dis,N}$) and without $NaBH_3CN$ ($k_{dis,X}$). (**C**) Formation rates of DPC_{in} in the presence of $NaBH_3CN$. (**D**) Zoom-in view of the locations of E187, K186, and two AP sites in the crystal structure of TFAM (PDB:3TQ6). For comparison, two AP positions were shown in the same crystal structure. (**E**) Comparison of k_{dis} under different reaction conditions with AP_{17} or AP_{20}. Data were averages with S.D. (n=3).

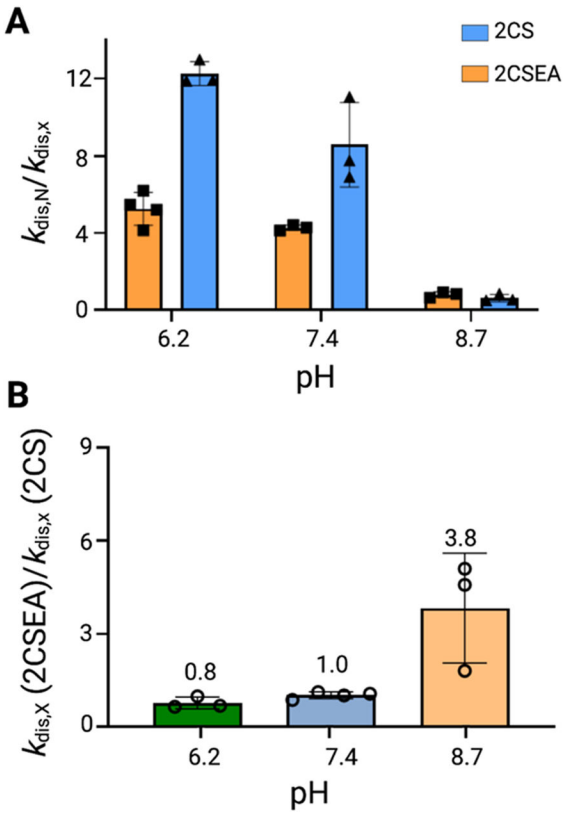

Figure 4.

Comparison of the kinetics of AP-DNA scission by TFAM under different pH conditions. (**A**) Ratios of the rate of AP-DNA disappearance with ($k_{dis,N}$) and without NaBH3CN ($k_{dis,X}$) for 2CS and 2CSEA. (**B**) The ratios of $k_{dis,X}$ of 2CSEA divided by $k_{dis,X}$ of 2CS under different pH conditions. Data are average values. Errors are S.D. (n=3).

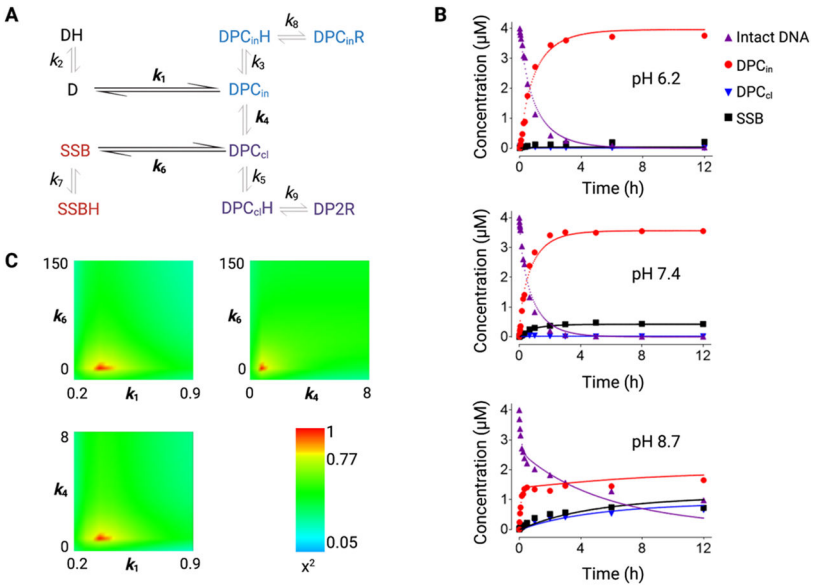

Figure 5.

Global data analysis and kinetic simulations of TFAM-catalyzed AP-DNA strand scission under three pH conditions. (**A**) Simplified kinetic model for reactions in the presence of $NaBH_3CN$. The model for reactions in the absence of $NaBH_3CN$ contains similar steps except without steps forming DP1R (step 8) and DP2R (step 9). (**B**) Global fitting of data obtained under pH 6.2, 7.4, and 8.7. (**C**) FitSpace contour analysis demonstrates that the Schiff-base formation (k_1), β-elimination (k_4), and dissociation (k_6) were well constrained by data. Couture plots show k_1, k_4 and k_6 as a function of each other. The Chi^2 boundary of each parameter was set at 0.833.

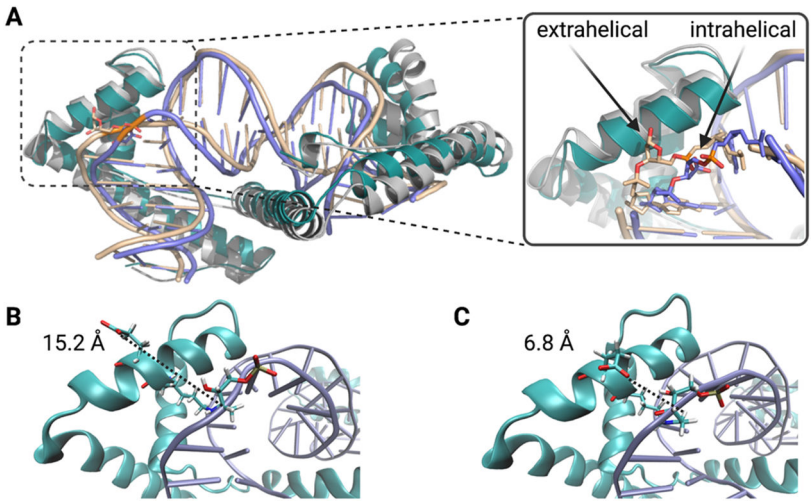

Figure 6.

Conformational dynamics of AP sites and E187 obtained by MD simulations. (**A**) Representative intrahelical (purple) and extrahelical (wheat) conformations of the AP lesion site observed in MD simulations. In (**B**) and (**C**), the Schiff base was modeled in the TFAM-DNA complex. Two simulation frames show (**B**) the farthest distance (186 ns) and (**C**) the closest distance (163 ns) between the proximal O atom of E187 side chain and the C1′ hydrogen in angstrom.

Table 1.

The rate of AP-DNA disappearance (k_{dis}) and DPC yields in TFAM-mediated AP-DNA strand scission. Reactions were carried out with AP_{17} (4 μM) and TFAM (8 μM) for 12 h with or without $NaBH_3CN$. Details are described in Experimental Procedures. Data are average values ± S.D. (n≥3).

TFAM variants	$NaBH_3CN$	AP-DNA disappearance k_{dis} (10^{-5} s^{-1})	Total DPC yield (%)	DPC_{in} yield (%)	DPC_{cl} yield (%)
WT	−	5.1 ± 0.6	83 ± 3.6	0.04 ± 0.03	85 ± 3.4
	+	18 ± 2.2	92 ± 3.9	76 ± 4.0	16 ± 3.2
2CS	−	5.2 ± 0.9	71 ± 2.7	1.6 ± 0.5	70 ± 3.2
	+	23 ± 2.3	99 ± 0.1	76 ± 6.3	24 ± 6.2
2CSEA	−	5.5 ± 1.3	80 ± 5.5	1.4 ± 0.4	79 ± 5.8
	+	44 ± 2.2	100 ± 0.1	89 ± 2.0	11 ± 2.0

Table 2.

TFAM-catalyzed AP-DNA cleavage reaction with AP_{17} in 12-h reactions under different pH conditions. Data are average values ± S.D. (n≥3). $k_{dis,N}$ is the rate of AP-DNA disappearance in the presence of $NaBH_3CN$; $k_{dis,X}$ is the rate of AP-DNA disappearance in the absence of $NaBH_3CN$.

pH	TFAM	$NaBH_3CN$	$t_{1/2}$ (h)	AP-DNA disappearance k_{dis} (10^{-5} s^{-1})	$k_{dis,N}/k_{dis,X}$
6.2	2CS	+	1.1 ± 0.2	19 ± 1.5	5.6 ± 0.5
		−	5.7 ± 0.9	3.4 ± 0.5	
	2CSEA	+	0.6 ± 0	32 ± 1.6	12 ± 0.6
		−	7.5 ± 0.6	2.6 ± 0.2	
7.4	2CS	+	0.8 ± 0.1	23 ± 2.9	4.3 ± 0.1
		−	3.8 ± 0.6	5.2 ± 0.9	
	2CSEA	+	0.4 ± 0	44 ± 2.2	8.6 ± 2.2
		−	3.6 ± 0.8	5.5 ± 1.3	
8.7	2CS	+	0.6 ± 0.1	35 ± 4.5	0.8 ± 0.1
		−	0.4 ± 0.1	44 ± 6.2	
	2CSEA	+	0.2 ± 0	96 ± 15.3	0.6 ± 0.2
		−	0.1 ± 0.1	162 ± 61	

Table 3.

Effects of TFAM variants on the half-life ($t_{1/2}$) of AP-DNA. The $t_{1/2}$ of AP-DNA was obtained under the same assay conditions as TFAM reactions except without TFAM. The fold reduction was calculated based on the ratios of $t_{1/2}$ of free AP_{17} divided by $t_{1/2}$ of AP_{17} in DNA-TFAM reactions in the absence of $NaBH_3CN$. Data under pH 7.4 are average values ± S.D. (n=3). Data obtained under pH 6.2 and pH 8.7 are average values ± range of data (n=2).

	$t_{1/2}$ (h) of free AP-DNA	**Fold reduction in $t_{1/2}$ relative to 2CS**	**Fold reduction in $t_{1/2}$ relative to 2CSEA**
pH 6.2	630 ± 37	110	84
pH 7.4	393 ± 78	103	109
pH 8.7	69 ± 7	173	690

Table 4.

TFAM-facilitated AP-DNA cleavage with AP_{17} in a 12-h reaction under pH 6.2, 7.4 and 8.7. Summary of DPC formation comparison from kinetic parameters including DPC_{in} yield, DPC_{cl} yield, and the ratio between DPC_{in}/DPC_{cl} after 12 h. The percent yield is calculated based on the sum of remaining AP_{17}, DPC_{in}, DPC_{cl}, and SSBs. Data are average values ± S.D. (n≥3).

pH	TFAM	$NaBH_3CN$	DPC_{in} (%)	DPC_{cl} (%)	DPC_{in}/DPC_{cl}
6.2	2CS	+	80 ± 5.3	16 ± 4.2	5.3 ± 1.5
		−	0.6 ± 0.2	66 ± 1.1	0.01 ± 0.003
	2CSEA	+	94 ± 3.4	5.2 ± 3.1	29 ± 27
		−	1.4 ± 1.2	54 ± 5.3	0.03 ± 0.03
7.4	2CS	+	77 ± 4.0	24 ± 6.2	3.3 ± 1.1
		−	1.6 ± 0.5	70 ± 3.2	0.02 ± 0.01
	2CSEA	+	89 ± 1.9	11 ± 2.0	8.5 ± 1.7
		−	1.4 ± 0.4	79 ± 5.8	0.02 ± 0.01
8.7	2CS	+	27 ± 5.6	44 ± 4.0	0.6 ± 0.1
		−	2.1 ± 0.2	56 ± 3.8	0.1 ± 0.04
	2CSEA	+	41 ± 0.7	18 ± 8.8	2.9 ± 2.0
		−	12 ± 11	29 ± 7.9	0.8 ± 0.7

Table 5.

Simulated parameters for Schiff-base formation, β-elimination and dissociation reactions with 2CS and 2CSEA and AP_{17}. Errors are S.E. from simulations from KinTek Explorer.

Steps	TFAM	$NaBH_3CN$	Lower bound	Upper bound	Best-fit values
k_1 (μM^{-1} h^{-1}) forward, Schiff-base formation	2CS	+	0.13	0.21	0.16 ± 0.04
		−	0.05	0.09	0.07 ± 0.01
	2CSEA	+	0.34	0.47	0.39 ± 0.06
		−	0.05	0.12	0.09 ± 0.03
k_{-1} (h^{-1}) reverse, Schiff base formation	2CS	+	1.3	5.6	2.5 ± 1.7
		−	2.1×10^{-9}	2.1×10^{-6}	2.1×10^{-7}
	2CSEA	+	0.34	0.47	4.3 ± 1.2
		−	4.0×10^{-9}	4.0×10^{-6}	4.0×10^{-7}
k_4 (h^{-1}) forward, β-elimination	2CS	+	1.3	5.0	2.5 ± 1.6
		−	1.3	2.5	1.6 ± 0.46
	2CSEA	+	0.50	1.2	0.78 ± 0.37
		−	0.68	1.3	0.85 ± 0.24
k_{-4} (h^{-1}) reverse, β-elimination	2CS	+	24	120	59
		−	8.1×10^{-9}	8.1×10^{-6}	8.1×10^{-7}
	2CSEA	+	24	110	58.2
		−	1.7×10^{-10}	1.7×10^{-7}	1.7×10^{-8}
k_6 (h^{-1}) forward, TFAM dissociation	2CS	+	11	17	14 ± 4
		−	0.04	0.08	0.05 ± 0.01
	2CSEA	+	10	20	16 ± 6
		−	0.05	0.07	0.06 ± 0.03
k_{-6} (h^{-1}) reverse, TFAM dissociation	2CS	+	6.9×10^{-9}	6.9×10^{-6}	6.9×10^{-7}
		−	8.9×10^{-12}	8.9×10^{-9}	8.9×10^{-10}
	2CSEA	+	1.2×10^{-10}	1.2×10^{-7}	1.2×10^{-8}
		−	6.9×10^{-10}	6.9×10^{-7}	6.9×10^{-8}